JSR Publications

Available Online

J. Sci. Res. **7** (1-2), 23-34 (2015)

JOURNAL OF SCIENTIFIC RESEARCH

www.banglajol.info/index.php/JSR

Effect of N and Cu Doping on Structure, Surface Morphology and Photoluminescence Properties of ZnO Thin Films

M. N. H. Liton[a,b], M. K. R. Khan[b*], M. M. Rahman[b], M. M. Islam[c]

[a,b]Department of Physics, Begum Rokeya University, Rangpur -5400, Bangladesh

[b]Department of Physics, University of Rajshahi, Rajshahi-6205, Bangladesh

[c]Atomic Energy Commission, Agargaon, Dhaka-1207, Bangladesh

Received 18 July 2014, accepted in final revised form 25 March 2015

Abstract

Thin films of ZnO, ZnO:Cu, ZnO:N and ZnO:(Cu,N) have been deposited on glass substrate at temperature 350ºC by low cost spray pyrolysis (SP) technique at an ambient atmosphere. The X-ray diffraction (XRD) study revealed that the films are of mono-phasic polycrystalline in nature having wurtzite ZnO crystal structure. The preferential orientation of un-doped ZnO films is in the (002) plane which changes to (101) for N and Cu mono-doped and (Cu, N) co-doped ZnO films. Surface morphology studied by scanning electron microscopy (SEM) clearly shows the formation of rock shaped nanostructures and hexagonal crystalline grains. The atomic force microscopy (AFM) study revealed the formation of crystalline grains perpendicular to the surface and reduction of surface roughness with doping. The photoluminescence (PL) spectra of the un-doped and doped ZnO samples show well defined transitions of the near band edge (NBE) and deep level (DLE) emissions emerged from different defect states present in the films.

Keywords: ZnO; Surface Morphology; Spray pyrolysis; Photoluminescence.

doi: http://dx.doi.org/10.3329/jsr.v7i1-2.19573 J. Sci. Res. **7** (1), 23-34 (2015)

1. Introduction

Nowadays, ZnO is an important multifunctional material which gained attractive attention due to self-assembled growth of three-dimensional nano-scale systems. The subtle interplay between its structure and physical properties yields prospects in microelectronic and shortwave optoelectronics applications. ZnO semiconductor has a direct band gap of 3.37 eV which crystallizes in hexagonal Wurtzite structure [1] and its space group is $P6_3mc$ and cell parameters are a = 0.3249 nm and c = 0.5206 nm [2]. It has high exciton binding energy (60 meV), which ensures efficient excitonic emission even at room

* *Corresponding author*: fkrkhan@yahoo.co.uk

temperature and it also leads to lasing action based on exciton recombination even above room temperature. Moreover, many important properties of ZnO is related with its morphology; such as nanostructure grain size of ZnO film can be exploited for improving the performance of various optoelectronic devices. Owing to these properties, ZnO has gained substantial attention as a promising candidate for potential applications in optoelectronic devices such as blue- and ultraviolet (UV)- light emitting diodes, varistors, transparent high-power electronics, surface acoustic wave devices, piezoelectric transducers, gas-sensing, window materials for display and solar cells [3-5]. Furthermore, ZnO is used as semiconducting multilayer, photo-thermal conversion system, gas sensor and optical positions sensors etc. [6].

Different methods of growing ZnO thin film with consistent morphology, crystalline quality and reproducible optical properties with long-term stability have been tried in the past; such as sputtering [7-8] thermal evaporation [9] and spray pyrolysis [10-11]. Among these, spray pyrolysis is a very simple and cost effective as it does not require a vacuum apparatus. Another advantage of the spray pyrolysis technique is that it can be adapted easily for production of large-area films to use in display manufacturing. It should be noted that the efficiency and performance of optical and electrical nano-devices are related to the crystallographic orientation, size, shape, surface morphology of the films. In this work, we focused on doping dependent change of crystallographic orientation and its consequences of ZnO nano-crystalline thin films and studied the effects of N and Cu doped on microstructures, surface morphology and photoluminescence properties of nano-structured ZnO thin films.

2. Experimental

ZnO, ZnO:Cu, ZnO:N and ZnO:(Cu,N) thin films were deposited on glass substrate by spray pyrolysis (SP) technique at 350°C at an ambient atmosphere. The details of spray pyrolysis are given elsewhere [11]. Three kinds of aqueous solutions, viz., zinc acetate, ammonium acetate and copper chloride are chosen as the source of Zn, N and Cu, respectively. The concentration of the solutions was 0.1 mol/L. The films were produced at constant atomic ratio (3 at % N) of Cu and N. The possible chemical reactions that occurred on the heated substrate to produce ZnO and Cu, N doped ZnO films are as follows:

$$(CH_3COO)_2Zn.2H_2O \xrightarrow{350\ ^\circ C} ZnO + CO_2\,(g) + CH_4\,(g) + \text{Steam (g)}$$

$$(CH_3COO)_2Zn.2H_2O + CH_3COONH_4 \xrightarrow[\text{Decomposes to}]{350\ ^\circ C} ZnO{:}N + CO_2\,(g) + CH_4\,(g) + \text{Steam(g)}$$

$$(CH_3COO)_2Zn.2H_2O + CuCl_2 \xrightarrow[\text{Decomposes to}]{350\ ^\circ C} ZnO{:}Cu + Cl_2\,(g) + CO_2\,(g) + CH_4(g) + \text{Steam (g)}$$

$$(CH_3COO)_2Zn.2H_2O + CuCl_2{+}CH_3COONH_4 \xrightarrow[\text{Decomposes to}]{350\ ^\circ C} ZnO{:}(Cu, N) + Cl_2\,(g) + CO_2\,(g) + CH_4\,(g) + \text{Steam (g)}$$

The XRD patterns of un-doped and doped ZnO films were taken with a diffractometer, (X'Pert PRO XRD PW 3040: angular resolution 0.001°). The diffraction scan was recorded within $20° \leq 2\theta \leq 60°$ of 2θ value using Cu K_α radiation (λ = 0.15405 nm) originate from a power source of 40 kV-30 mA. The crystallite size in the direction perpendicular to the substrate was determined from the peak width of the corresponding reflection by the Scherrer's formula.

The surface morphologies of un-doped and doped ZnO films were studied by atomic force microscopy (AFM) (XE70 PARK SYSTEMS) and scanning electron microscopy (SEM) (FEI QUANTA INSPECT S50). The room temperature photoluminescence (RTPL) spectra were taken by Spectrofluorophotometer (RF-5301PC).

3. Results and Discussions

The XRD patterns of un-doped and doped ZnO films are shown in Fig. 1. XRD pattern clearly shows that ZnO thin film deposited by SP method is single phase polycrystalline in nature. The observed reflection planes (100), (002), (101), (102) and (110) could be indexed with hexagonal ZnO structure which was identified by comparing with standard JCPDS card (Card no. 2100100). No trace of phases like Zn_3N_2, CuO or Cu- metal other than ZnO were confirmed, which indicate that Cu and N atoms are inserted in ZnO lattice and are not isolated from ZnO matrix.

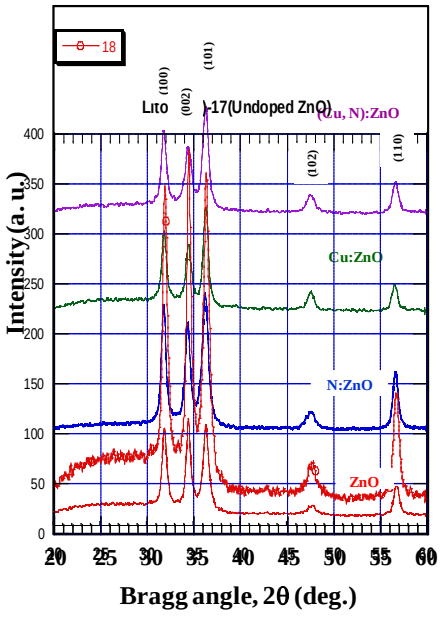

Fig. 1. XRD patterns of un-doped, N doped, Cu doped and (Cu, N) co-doped ZnO films.

Fig. 1 also shows that the peak intensity of (002), (100) and (101) planes are dominating both for un-doped and doped samples. For un-doped sample the peak intensity of (002) plane is higher than that of other two planes. However, the intensity of (002) plane for doped samples is found lower compared to (100) and (101) planes. It is also noticed that the XRD intensity is highest for N doped ZnO sample compared to other samples. These results suggests that the preferential orientation of un-doped sample is in the (002) plane. The N and Cu doping in the ZnO lattice induced the change of preferential orientation from (002) plane to (101) plane. The change in crystallographic orientation with the effect of Cu and N doping in ZnO suggests that the orientation energy is lower in (101) plane compared to (002) plane. As a result, crystal grains are oriented along (101) plane for doped samples. It seems that the microstructure of the ZnO lattice changes due to the doping effect that inevitably perturbed the thermodynamic energy in the system that may create probability to change the preferable orientation.

From XRD patterns of Fig.1, it is seen that the peak positions shift with N, Cu and (Cu, N) co-doping in ZnO. The peak positions of (002) plane for ZnO, N-doped ZnO, Cu-doped ZnO and (Cu, N) co-doped ZnO samples are 34.437, 34.339, 34.443, 34.335 and for (101) plane are 36.308, 36.185, 36.281, 36.252 degrees respectively. From these data it is seen that with N, Cu, (Cu, N) co-doping the peak positions of (002) and (101) planes shift slightly toward lower angle compared to un-doped ZnO crystal except Cu doping where the peak position of (002) plane shifts toward slightly higher angle. An angular shift of 0.08° in (002) plane was reported [12] for N doped ZnO crystal. The obtained XRD results can be explained as: in the case of N-doping, N atom may substitute O atom and at the same time it may sits in the interstitial position in covalent bond of ZnO crystal. The covalent radius of N (0.075 nm) is higher than that of O (0.073 nm). In this case, they create extra stress in the lattice and as a result it leads to increase in inter-planar distance and subsequently peak positions shifted to lower angles. The same scenario happens for Cu doping in ZnO crystal. Here Cu (0.138 nm) atoms substitute Zn (0.131 nm) atoms. The effect of N doping on stress is higher than other doping atoms as shown in Table 1. This happens due to the possibility of occupying interstitial positions by N in ZnO lattice. However, for (Cu, N) co-doping the effect is less than N doping but higher than Cu doping. As a result, the intensity of (002) plane is lower for Cu doping in ZnO crystal than that of un-doped ZnO crystal and in this case the preferred orientation changes to the (101) plane. This may lead to the decrease in compressive stress in the (002) plane and as a result peak positions shift more to the higher angle for doped samples compared to un-doped ZnO. Due to the overall effect of N, Cu and (Cu, N) co-doping the lattice parameters are expected to increase slightly in doped samples.

The lattice parameters *a* and *c* for hexagonal structure was calculated using the following equation [13],

$$\frac{1}{d_{hkl}^2} = \frac{4}{3}\left\{\frac{(h^2+hk+k^2)}{a^2}\right\} + \frac{l^2}{c^2} \quad (1)$$

The calculated lattice parameters for N and Cu doped and (Cu, N) co-doped ZnO films are given in Table 1. The estimated lattice parameters of doped and co-doped ZnO films become higher than un-doped ZnO films as expected that indicates Cu and N forms ZnO solid solution.

Table 1. Lattice constant, average crystallite size, dislocation density, strain and stress of un-doped and doped ZnO thin films.

Type of doping	Lattice constant		c/a ratio	Average crystallite size, ζ (nm)	Dislocation Density, δ ($x10^{15}m^{-2}$)	Strain, ε_z (%)	Strained Stress, σ_{film} (GPa)
	a (nm)	c (nm)					
Un-doped ZnO	0.3245	0.5209	1.605	24	1.74	0.08	– 0.35
N doped ZnO	0.3248	0.5208	1.603	29	1.19	0.06	– 0.25
Cu doped ZnO	0.3256	0.5223	1.604	19	2.77	0.35	– 1.58
(Cu, N) co-doped ZnO	0.3257	0.5224	1.604	20	2.50	0.37	– 1.66

The average size of crystallites was estimated by using the Debye-Scherrer formula:

$$\xi = \frac{0.94\lambda}{\beta cos\theta} \quad (2)$$

where, ξ is the crystallite size, λ is the wavelength of the X-ray used, θ is the diffraction angle and β is the full width at half maximum (FWHM) measured in radians. The calculated crystallite size or grain size for N and Cu doped and (Cu, N) co-doped ZnO films are also included in Table 1. From Table 1 it is observed that the average grain size along the *c*-axis slightly affected by Cu and N doping in ZnO.

The texture coefficient $T_{c\ (hkl)}$ is a parameter that solely governed the preferential orientation of a crystal has been calculated for (100), (002) and (101) planes using the expression [14]

$$T_{c(hkl)} = \frac{\frac{I_{hkl}}{I_{r(hkl)}}}{\frac{1}{n}\left(\sum \frac{I_{hkl}}{I_{r(hkl)}}\right)} \quad (3)$$

where $I_{r\ (hkl)}$ is the intensity of the reference (*hkl*) plane, $I_{\ (hkl)}$ is the observed intensity of the (*hkl*) plane and *n* is the number of diffraction peaks. The calculated $T_{c\ (hkl)}$ values of different planes are shown in Table 2. The value $T_c\ (hkl) = 1$ represents films with randomly oriented crystallites, while higher values indicate the abundance of grains oriented in a given (*hkl*) direction. From Table 2, it is seen that the values of $T_{c(hkl)}$ are greater than 1 for (100), (002) and (101) planes that indicates grains are oriented in these planes. However, the values of $T_{c(hkl)}$ for (101) plane are higher than that of (100) and (002) planes for doped samples implies the preferred orientation is in (101) plane

Table 2. The texture coefficient, $T_{c(hkl)}$ of major (hkl) planes of un-doped and doped ZnO thin films.

Type of doping ↓	Texture coefficients (hkl) → (100)	(002)	(101)
Un-doped ZnO	1.34	1.56	1.48
N doped ZnO	1.41	1.19	1.54
Cu doped ZnO	1.28	1.08	1.83
(Cu, N) co-doped ZnO	1.32	1.05	1.79

In tetrahedral geometry of ZnO, there are three lowest density of the surface free energy viz., 9.9, 12.3 and 20.9 eV/nm^2 corresponding to (002), (101) and (100) planes [15]. Therefore, the films are commonly (002) textured due to its low surface free energy. But the surface free energy of the (002) plane is not necessarily always smaller than those of other planes [16]. If a film is grown at low temperature and if a large density of defect impurities exists in films then other orientations are also possible [17]. The temperature dependency of crystal orientation is reported for ZnO films [18]. In this study, we found doping dependent change of crystal orientation for ZnO films grown at a constant temperature 350°C. The preferential orientation of (002) plane of ZnO changes to (101) plane in case of N and Cu doped and (Cu, N) co-doped ZnO films. Therefore, this change of orientation is certainly as the effect of N and Cu doping in ZnO lattice. Similar result was observed for indium doped ZnO thin films [19].

The lattice strain also affects the structures and properties of ZnO films to some extent and the average uniform strain ε_z has been calculated from the lattice parameters using the following expression:

$$\varepsilon_z = \left(\frac{c - c_0}{c_0}\right) \times 100\% \tag{4}$$

where, c_o is the un-strained standard lattice constant of ZnO (0.5206 nm) and c is the strained lattice constant of doped ZnO films under study prepared by spray pyrolysis. The values of ε_z are included in Table 1.

For hexagonal crystal, the stress, σ_{film} in the plane of the film can be calculated by using biaxial strain model [20] given as,

$$\sigma_{film} = \frac{2C_{13}^2 - C_{33}(C_{11} + C_{12})}{C_{13}} \varepsilon_z \tag{5}$$

where, C_{11} = 209.7 GPa, C_{12} = 121.1 GPa, C_{13} = 105.1 GPa and C_{33} = 210.9 GPa. The calculated stress for un-doped and Cu, N doped ZnO films are given in the same Table 1. It is found that the stress is strongly dependent on doping element. It is well-known from literature that there are, in general, two types of stress interplay in thin film. First one is the intrinsic stress introduced by impurities, defects and lattice distortions in the crystal

and the second is the extrinsic stress introduced by the mismatch between thermal expansion coefficients between the film and substrate. Obviously strain could be positive (tensile) or negative (compressive) according to the above Eq. (5). From Table 1, it is seen that all the samples have a positive strain, which may be due to the fact that Cu and N doping atoms can occupy some interstitial positions and substitute some oxygen vacancies as discussed earlier. Therefore, tensile strain is produced due to the doping and the lattice mismatch between the film and the substrate.

Surface morphology of un-doped and doped ZnO films is studied by scanning electron microscopy (SEM) and the SEM images are shown in Figs. 2(a-d). The SEM micrographs show strong dependency on doping elements. It is seen that hexagonal crystal grains with few voids are evident for ZnO and N-doped ZnO samples. For ZnO sample crystal grains are almost equal in size while a few bigger agglomerated crystal grains are distributed over the whole surface along with smaller one for N-doped sample. A rock shaped nano-slabs of hexagonal structure is observed for Cu doped ZnO crystal while (Cu, N) co-doped sample revealed the formation of clusters of hexagonal crystals distributed over whole surface.

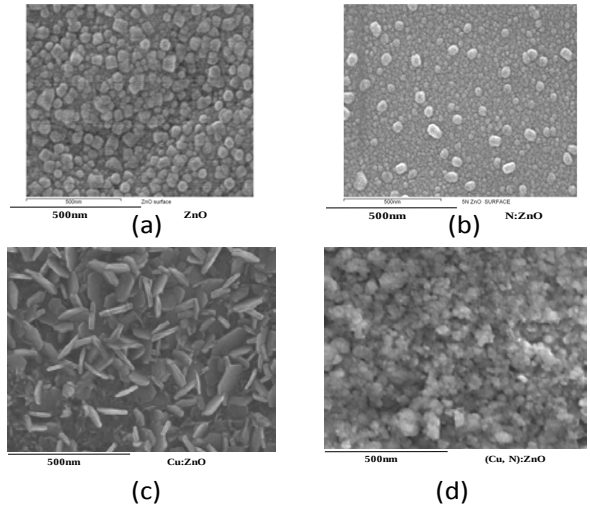

Fig. 2. SEM micrographs of ZnO films: (a) un-doped (b) N doped (c) Cu doped and (d) (Cu, N) co-doped.

The 2D- and 3D- AFM micrographs are shown in Figs. 3 and 4, respectively. The AFM image shows that the surface morphology is changed with the doping of different elements and the crystal grains possesses hexagonal symmetry. The images show differences in grain size consistent with the XRD measurements. Several needle-shaped nano-grains are thought to combine to form larger crystalline grains which expand the surface area of the crystals. From the AFM study, it is also found that the average surface roughness, R_a of the films are 0.317 nm, 0.01 nm, 0.081 nm and 0.083 nm for un-doped,

N doped, Cu doped and (Cu, N) co-doped ZnO films respectively. Therefore, roughness is reduced by doping different elements in ZnO films.

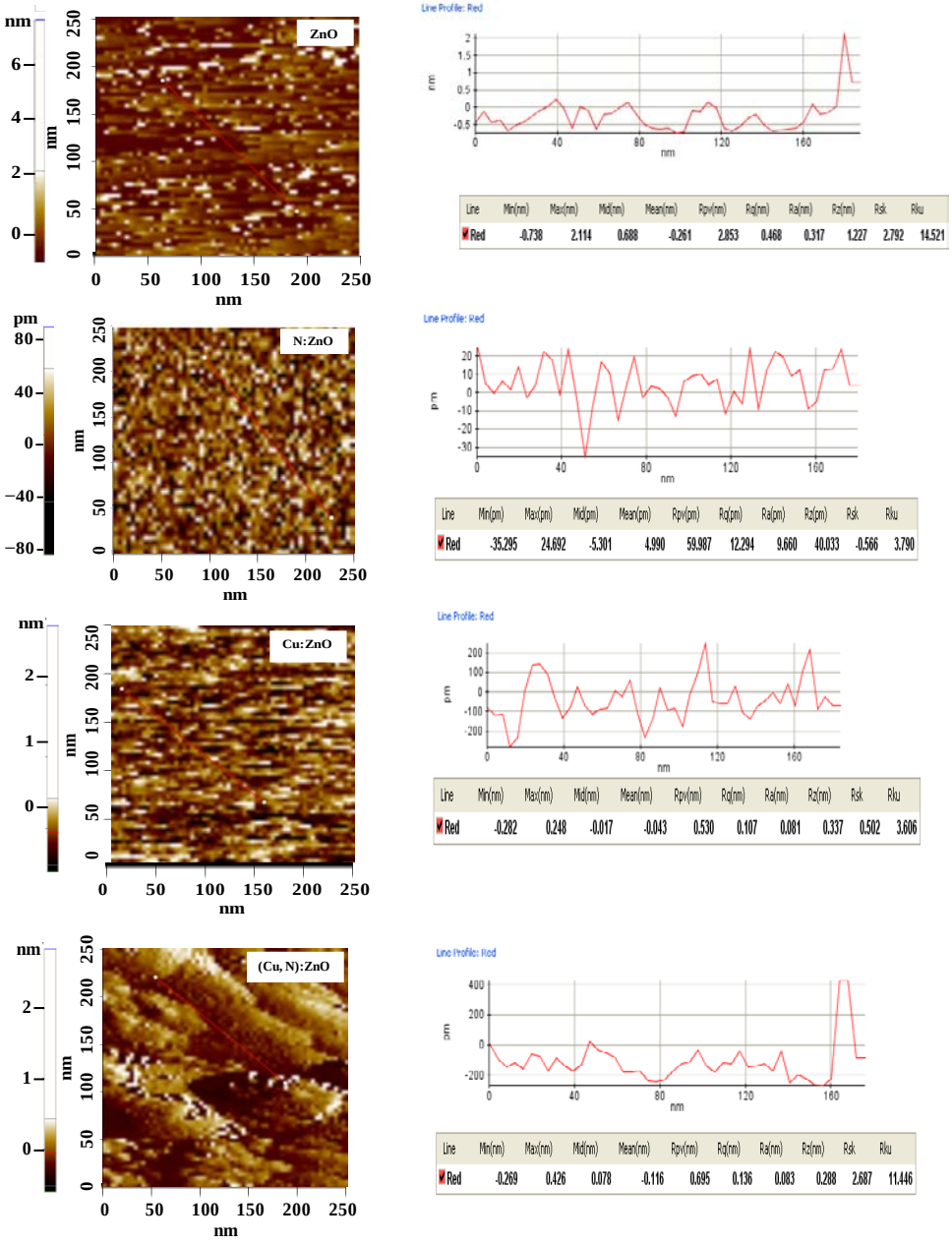

Fig. 3. 2-dimentional AFM images with line profile of ZnO films: (a) un-doped, (b) N doped, (c) Cu doped and (d) (Cu, N) co-doped.

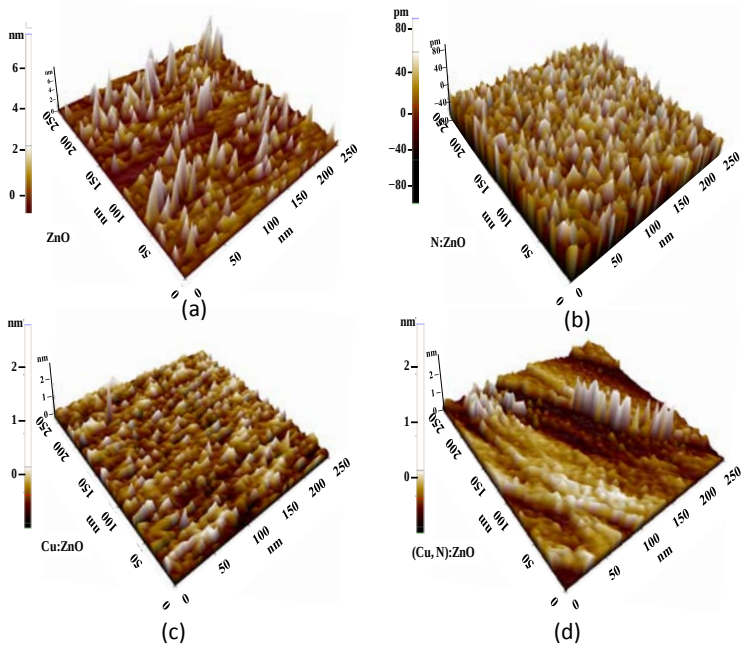

Fig. 4. 3-dimentional AFM images of ZnO films:(a) un-doped, (b) N doped, (c) Cu doped and (d) (Cu, N) co-doped.

The photoluminescence (PL) spectra at room temperature for un-doped and doped ZnO samples at excitation wavelength, λ_{ex}= 300 nm (4.133 eV) is shown in Fig. 5a. From figure it is seen that a dominant PL peak arises at 'a' [~ 365 nm (3.4 eV)], and some minor peaks arise at 'b' [~ 451 nm (2.76 eV)], 'c' [~ 469 nm (2.65 eV)],'d' [~ 482 nm (2.58 eV)] and 'e' [~ 493 nm (2.53 eV)]. For Cu, N and (Cu, N) co-doped ZnO samples the maxima of major peaks slightly shifted towards higher energy and the peaks broadened due to the doping. The slight variation in the PL peak intensity and positions were observed. The PL intensity of N doped ZnO sample is highest while the Cu doped and (Cu, N) co-doped ZnO samples PL intensity is lower compared to un-doped sample.

The PL transitions observed in this study can be explained as in the following: in general PL transitions are occurred mainly by four possible ways; i) band to band transition, ii) band to ionization state (donor or acceptor); iii) impurity band (donor-acceptor) transition and iv) deep level transitions. The quantitative analysis of these transitions for ZnO and doped (Cu, N) ZnO crystals are reported. The near band edge or direct band to band transition energy for undoped ZnO is 3.3 eV [21, 22]. The shallow defect state energy (V_o) due to O vacancies are at (0.5-0.7) eV bellow the bottom of conduction band [23, 24] and hence the corresponding band to ionization transitions energies would be (2.6-2.8). For complex defect energy states due to doping of donor and acceptor are located around (0.3-0.4) eV below the bottom of conduction band for donor

(V_o, N) [25] and at ~0.45 eV above the top of the valence band for acceptor (Cu+, h) [26] and their corresponding transition energy is ~2.55eV. Many researchers also believe the presence of Zn vacancy in the ZnO lattice at the energy state `0.8eV above the top of the valence band with green band energies associated in region of (2.4-2.6) eV [2, 27]. However, Xu *et al*. [28] reported the position of Zn vacancy (V_{Zn}) is at energy level ~0.3 eV above the top of valence band and hence their corresponding transition energies is [3.3eV-(0.3+0.3)eV] ~2.7 eV for donor-acceptor transition and [3.3 eV-(0.3+0.5) eV]~2.5eV for acceptor-ionization transition. In this study, the transition energies for the observed PL peaks at a, b, c, d and e are very similar to the above reported values. It should be noted that for co-doping of Cu and N in ZnO, all the possible PL transitions may be happened. From above analysis we propose the PL transition energy diagram on the basis of experimental obtained energies for Cu, N co doped ZnO crystals as shown in Fig. 5b. In this diagram, *Vo* represents ionization energy state due to oxygen vacancy in the lattice, N represents donor in the interstitial position, Cu+ for energy state of acceptor due to substitution of Cu ions and h represents holes due to substitution of oxygen by N ions.

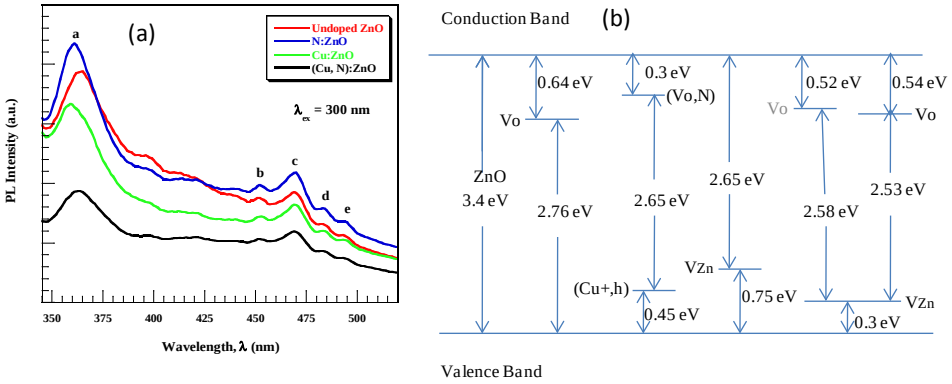

Fig. 5. PL spectra of un-doped, Cu and N-doped (a), energy levels of defect states of Cu and N doped (b) ZnO crytals

4. Conclusion

ZnO, Cu and N doped ZnO thin films are deposited by spray pyrolysis method. The deposited films are of single phase polycrystalline with hexagonal structure as confirmed by XRD experiment. The preferred crystallographic orientation of ZnO in (002) plane changed to (101) by doping Cu and N or by (Cu, N) co-doping. Micro-structural study confirms the presence of tensile strain in the films. The SEM micrograph confirms the growth of rock shaped nano slabs for Cu doped ZnO samples while the hexagonal nano structures are evident for un-doped, N doped and (Cu, N) co-doped samples The film surface is affected by the type of doping elements and the crystalline grains are

perpendicular to the film surface as confirmed by AFM. A multiple emissions of photoluminescence in ultraviolet and green regions emerged from different defect states present in the films.

Acknowledgment

One of the authors M. N. H. Liton is thankful to the Ministry of Science and Information & Communication Technology (MOSICT) of Peoples Republic of Bangladesh for providing financial support. We gratefully acknowledge Bangladesh Atomic energy Commission (AEC) for providing XRD, and SEM facilities.

References

1. V. Srikant and D.R. Clarke, J. Appl. Phys. **83**, 5447 (1998). http://dx.doi.org/10.1063/1.367375
2. S. L. King and J. G. E. Gardeniers, Appl. Surf. Sci. **811**, 96 (1996).
3. D. C. Look, Mater. Sci. Eng. B **80,** 383 (2001). http://dx.doi.org/10.1016/S0921-5107(00)00604-8
4. R. Triboulet and J. Perriere, Prog. Cryst. Growth Charact. Mater. **47**, 65 (2003). http://dx.doi.org/10.1016/j.pcrysgrow.2005.01.003
5. S. J. Pearton, D. P. Norton, K. Ip, Y. W. Heo, and T. Steiner, Prog. Mater. Sci. **50**, 293 (2005). http://dx.doi.org/10.1016/j.pmatsci.2004.04.001
6. D. Brida, E. Fortunato, I. Ferreira, H. Aguas, and R. Martins, J. Non-Cryst. Solids **1272**, 299 (2002).
7. T. Manami, H. Nanto, and S. Takata, Jpn. J. Appl. Phys. L **280**, 23 (1984).
8. E. Fortunato, V. Assuncao, A. Gonc alves, A. Marques, H. Aguas, L. Pereira, I. Ferreira, and R.. Martins, Thin Solid Films **443**, 451 (2004).
9. A. Dutta and S. Basu, Mater. Chem. Phys. **41**, 34 (1993).
10. P. Nunes, B. Frenandes, E. Fortunato, P. Vilarinho, and R. Martins, Thin Solid Films **337**, 176 (1999). http://dx.doi.org/10.1016/S0040-6090(98)01394-7
11. M. K. R. Khan, M. A. Rahman, M. Shahjahan, M. M. Rahman, M. A. Hakim, D. K. Saha, and J. U. Khan, Current Appl. Phys. **10**, 790 (2010). http://dx.doi.org/10.1016/j.cap.2009.09.016
12. K. Jindal, M. Tomar. R.S. Katiyar, and V. Gupta, J. Appl. Physics, **111**,102805 (2012). http://dx.doi.org/10.1063/1.4714686
13. B. D. Cullity and S. R. Stock, Elements of X-ray Diffraction (Prentice Hall, New Jersey, 2001) **388**, pp. 619.
14. C. Agashe, M. G. Takawale, B. R. Marathe, and V. G. Bhide, Sol. Energy Mater. **99**, 17 (1998).
15. N. Fujimura, T. Nishihara, S. Goto, J. Xu, and T. Ito, J. Cryst. Growth **130**, 269 (1993). http://dx.doi.org/10.1016/0022-0248(93)90861-P
16. H. N. Tran, A. J. Hartmann, and R. N. Lamb, J. Phys. Chem. B **103**, 4264 (1999). http://dx.doi.org/10.1021/jp9836426
17. J. Lu, Z. Ye, L. Wang, J. Huan, and B. Zhao, Mater. Sci. Semiconductor Process. **5**, 491 (2003). http://dx.doi.org/10.1016/S1369-8001(02)00114-2
18. A. Djelloul, and K. Bouzid, F. Guerrab, Turk. J. Phys. **32**, 49 (2008).
19. T. V. Vimalkumara, N. Poornimaa, K. B. Jineshb, C. S. Karthaa, and K. P. Vijayakumar, Appl. Surf. Sci. **257,** 8334 (2011). http://dx.doi.org/10.1016/j.apsusc.2011.03.118
20. C. Suryanarayana, M. G. Norton, X-Ray Diffraction-A Practical Approach (Plenum Press, New York and London, 1998). http://dx.doi.org/10.1007/978-1-4899-0148-4
21. E. Tomzig and R. Helbig J. Lumin. **14**, 403 (1976). http://dx.doi.org/10.1016/S0022-2313(76)91392-2
22. C. F. Klingshirn, Semiconductor Optics (Springer, Berlin, 1995).

23. F. Oba, S. R. Nishitani, S. Isotani, H. Adachi, and I. Tanaka, J. Appl. Phys. **90**, 824 (2001). http://dx.doi.org/10.1063/1.1380994
24. P. Erhart, K. Albe, and A. Klein, Phys. Rev. B **73**, 205203 (2006). http://dx.doi.org/10.1103/PhysRevB.73.205203
25. I. V. Rogozin, A. N. Georgobiani, M. B. Kotlyarevsky, and A. V. Marakhovskii, Inorg. Mater. **45**, 391 (2009). http://dx.doi.org/10.1134/S0020168509040116
26. A. Gupta, S. Kumar, and H. S. Bhatti, J. Mater. Sci.: Mater. Electron **21**, 765 (2010). http://dx.doi.org/10.1007/s10854-009-9990-4
27. X. Yang, G. Du, X. Wang, J. Wang, B. Liu, Y. Zhang, D. Liu, H. C. Ong, and S. Yang, J. Cryst. Growth **52**, 275 (2003). http://dx.doi.org/10.1016/S0022-0248(03)00898-4
28. P. S. Xu, Y. M. Sun, C. S. Shi, F. Q. Xu, and H. B. Pan, Nucl. Instrum. & Math. Phys. Res. B **199**, 286 (2003). http://dx.doi.org/10.1016/S0168-583X(02)01425-8